

The Spheroid Luminosity and Mass Functions From Hubble Space Telescope Star Counts

Andrew Gould*

Dept of Astronomy, Ohio State University, Columbus, OH 43210

Chris Flynn

Tuorla Observatory, Piikkiö, FIN-21500, Finland

John N. Bahcall

Institute For Advanced Study, Princeton, NJ

e-mail: gould@payne.mps.ohio-state.edu, cflynn@astro.utu.fi, jnb@ias.edu

Abstract

We analyze 166 spheroid subdwarfs ($6.5 < M_V < 14.5$) found in 53 fields observed with the Wide Field Camera on the *Hubble Space Telescope*. The fields cover 221 arcmin^2 over a wide range of directions. The spheroid luminosity function (LF) is inconsistent at about the 3σ level with the local spheroid LF of Dahn et al. even when the normalization of the latter is corrected to take account of the latest data on spheroid kinematics. The difference may reflect systematic errors in one of the two studies or features of the spheroid spatial distribution that are not included in the simplest models. The mass function, which shows no obvious structure, can be represented by a power law, $dN/d\ln M \propto M^\alpha$, with $\alpha = 0.25 \pm 0.32$ over the mass range $0.71 M_\odot > M > 0.09 M_\odot$. The spheroid therefore does not contribute significantly to microlensing unless the mass function changes slope dramatically in the substellar range. The total local mass density of spheroid stars (including remnants and unseen binary companions) is $\rho \sim 6.4 \times 10^{-5} M_\odot \text{ pc}^{-3}$, with an uncertainty of about 50%. The power-law indices $\alpha = 0.25$ for the spheroid and $\alpha = 0.44$ for the disk (both uncorrected for binaries) are similar to those of globular clusters of moderate to high metallicity.

Subject Headings: stars: low mass, luminosity function

* Alfred P. Sloan Foundation Fellow

1. Introduction

Subdwarfs comprise the great majority of stars in the Galaxy's spheroidal component. There are three main reasons to study the luminosity function (LF) and physical distribution of these objects.

First, microlensing results indicate that a substantial fraction of the Galaxy's dark matter may be in compact objects (Alcock et al. 1997). While spheroid stars themselves certainly cannot be responsible for the majority of the microlensing events (Bahcall et al. 1994, hereafter Paper I; Graff & Freese 1996; Reid et al. 1996; Flynn, Gould, & Bahcall 1996, hereafter Paper II; Méndez et al. 1997), it is possible that substellar objects in the spheroid do make a non-negligible contribution. The *shape* of the spheroid stellar LF and hence the shape of its stellar mass function (MF) provide an important clue by extrapolation to the density of these substellar spheroid objects (Méra, Chabrier, & Schaeffer 1996).

Second, by comparing the spheroid LF with that of globular clusters, one can gain insight into the evolution of the latter. Globular clusters appear to have anomalously low mass-to-light ratios compared to other old systems with dynamically measured masses such as elliptical galaxies and the bulges of spirals. A plausible explanation for this discrepancy is that the globulars have lost the majority of their initial mass by evaporation of their low-mass stars. If this explanation were correct, then one would expect the LF and MF of field stars to be rising more steeply toward low masses than the LFs and MFs of globular clusters.

Third, spheroid stars are an unwanted foreground in studies of extra-galactic objects, such as counts of faint galaxies. An accurate estimate of the spheroid stellar density is useful both for planning observations and for removal of this background (Bahcall 1986).

There are two basic approaches for determining the spheroid LF. The first, pioneered by Schmidt (1975), is to extract a local sample of spheroid stars from a proper-motion catalog, measure their parallaxes (and so their absolute magnitudes), and then estimate their density as a function of absolute magnitude. To avoid contamination by disk stars which are more numerous than spheroid stars in the solar neighborhood, it is necessary to set stringent kinematic selection criteria (Bahcall & Casertano 1986, hereafter BC). These criteria must then be properly modeled in order to extract the underlying LF from the observed counts. BC applied this method to 94 stars with transverse speeds $V_T > 220 \text{ km s}^{-1}$ taken from the Eggen (1979a, 1980) proper motion survey. The distances were determined photometrically based on Eggen's (1979b) linear color-magnitude relation. Dahn et al. (1995, hereafter DLHG) applied essentially the same method to a sample of 114 stars with $V_T > 220 \text{ km s}^{-1}$ taken from the Luyton (1979) proper

motion catalog and for which they obtained reliable trigonometric parallaxes. Because trigonometric parallaxes are fundamentally more reliable than photometric parallaxes and because the actual color-magnitude relation is neither linear nor one-to-one (Baraffe et al. 1997; and § 3.2, below) we compare our results primarily to DLHG. The DLHG LF peaks near $M_V = 11.5$, similar to the peak of the disk LF (Stobie, Ishida & Peacock 1989; Kroupa, Tout & Gilmore 1993; Reid, Hawley, & Gizis 1995; Gould, Bahcall, & Flynn 1996, 1997 – hereafter Papers III and IV.)

An alternative method is to determine the spheroid LF from star counts. The major difficulty of this approach has been that stars could be reliably distinguished from galaxies only to relatively bright magnitude limits, typically $V \lesssim 20$. At these magnitudes and for most colors, disk stars greatly outnumber spheroid stars and it is therefore difficult to isolate a spheroid sample. For this reason, Bahcall & Soneira (1980), when they first applied this method, restricted attention to blue stars near the main-sequence turn-off which are relatively isolated from the disk population in the color magnitude diagrams (CMDs) of the deepest ground-based images of the time. Richer & Fahlman (1992) extended this approach to redder subdwarfs by counting stars in a pair of deep CCD images at high Galactic latitude. They reported a LF that is steeply rising at faint magnitudes in sharp contrast to the LF of DLHG which falls in the same region. However, the faint end ($V - I > 1.75$) of the Richer & Fahlman (1992) spheroid sample is severely contaminated with disk stars (Reid et al. 1996).

Here we analyze star counts from 53 fields imaged with the Wide Field Camera (WFC2) on the repaired *Hubble Space Telescope (HST)*, covering a total area of 221 arcmin². One can unambiguously distinguish stars from galaxies in these fields to a mean limiting magnitude $I = 23.8$, several magnitudes fainter than is possible from the ground. This faint limiting magnitude provides two major advantages relative to ground-based measurements. First, one can measure the vertical profile of disk M stars and thereby determine the minimum magnitude (as a function of color) beyond which disk stars cease to be a serious contaminant. By establishing a “disk-free” threshold, one eliminates the largest potential source of systematic error, contamination at the red end by disk stars. One could in principle measure the vertical profiles of late G or K stars from the ground since these are substantially brighter. These profiles should be similar to that of M stars. However, for these earlier type stars, one risks contamination from evolved spheroid stars (Paper III). The second advantage is that one can search for spheroid stars for several magnitudes beyond this disk-free threshold, allowing one to determine the three-dimensional distribution of spheroid main-sequence stars for the first time.

We derive in this paper the spheroid LF over the range $6.5 < M_V < 14.5$. The LF is relatively flat or slightly rising over this range, in contrast to the spheroid

LF of DLHG which shows a distinct peak at $M_V \sim 12$ and also in contrast to several recently measured globular cluster LFs which peak near $M_V \sim 10$. We also derive a MF, which shows no obvious structure. We fit the MF to a power law $dN/d\ln M \propto M^\alpha$, and find $\alpha = 0.25 \pm 0.32$. We derive an empirical color-magnitude relation in order to be able to extract a LF from the photometric data. The MF should be interpreted more cautiously than the LF, since to extract a MF from photometric data one requires mass-luminosity and mass-color relations. While empirical mass-luminosity relations are available for disk stars (Henry & McCarthy 1993), none have been established for the spheroid. Hence, we rely on the purely theoretical calculations of Baraffe et al. (1997) for the mass-luminosity relation.

In § 2, we review the observations and data reduction. In § 3, we discuss our parameterization of the spheroid and our construction of a color-magnitude relation. In § 4, we extract the LF and MF from the data, and in § 5, we discuss some of the implications of these results.

2. Observations and Data Reduction

The sample is selected from the stars found in 53 fields with a total area of 221 arcmin² imaged with WFC2 on *HST*. The field centers and limiting magnitudes are given in Table 1 of Paper IV. The procedure for identifying stars and measuring their fluxes is summarized in Paper IV which refers to Papers I, II, and III for further details.

Figure 1 shows the $I, V - I$ CMD for the total of 166 stars that meet the two selection criteria described below. The selection criteria were devised so as to obtain a nearly pure sample of spheroid subdwarfs. First, we exclude disk dwarfs by demanding that the inferred distance from the Galactic plane (assuming a *disk* color-magnitude relation: $M_V = 3.37(V - I) + 2.89$) be at least 8 kpc. In Paper IV, we measured the vertical profile of disk stars (including both the thin-disk and intermediate populations). From Figure 1 of Paper IV, it is clear that few disk stars have inferred distances above 6 kpc. We nevertheless adopt a still more conservative limit of 8 kpc because disk stars are $\sim 10^3$ times more common than spheroid stars at the plane and so could be a serious contaminant even at relatively low densities. The disk stars need not actually be above 8 kpc to cause contamination: the intermediate disk population is more metal-weak and hence less luminous than the main disk population, so that the true distances may be as little as half the inferred distances for the most distant stars. Nevertheless, since it is the *inferred distances* that are shown in Figure 1 of Paper IV, the 8 kpc *inferred-distance* cutoff will remove essentially all disk stars. The diagonal line in

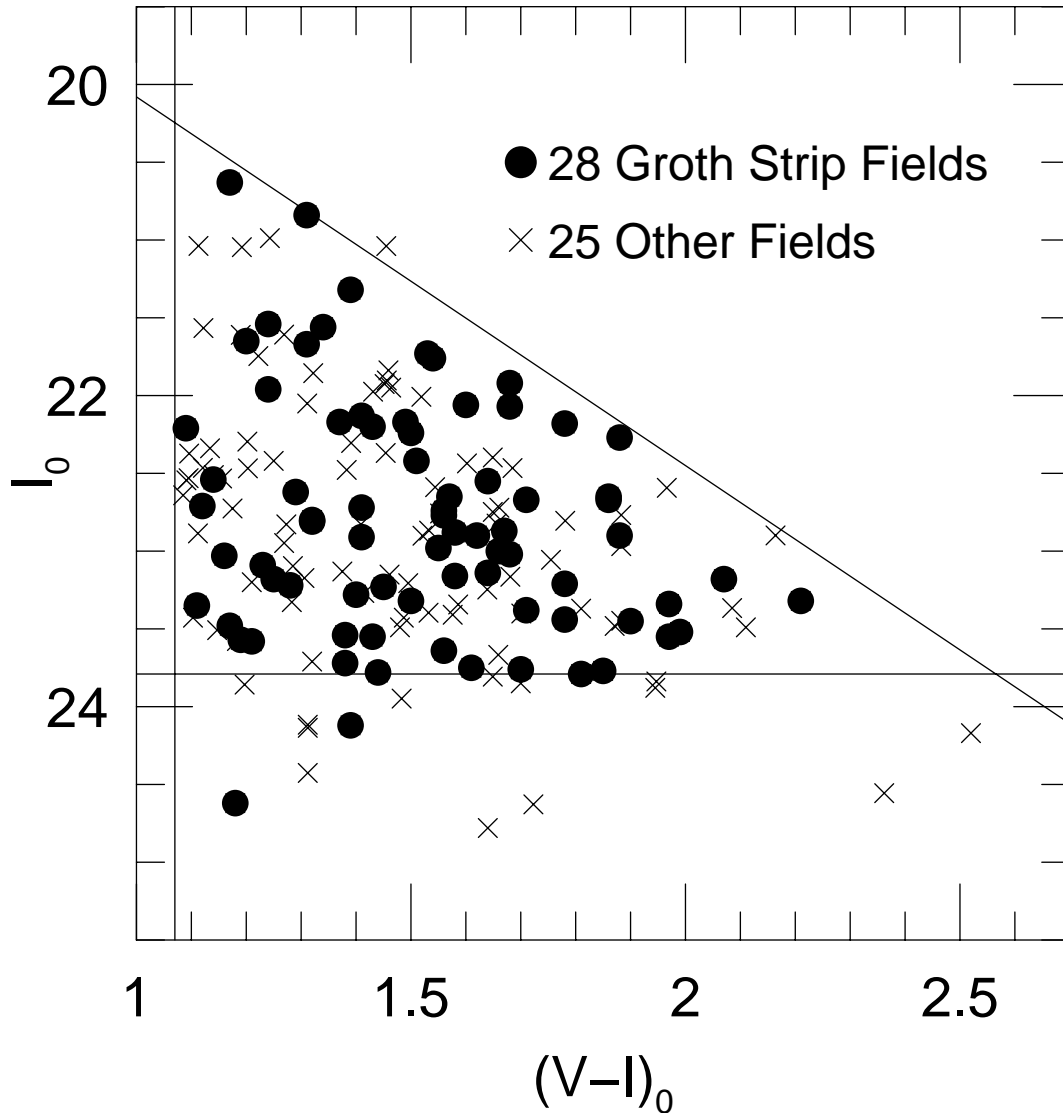


Figure 1. Dereddened CMD of 166 spheroid stars detected in 53 fields observed with the *HST* WFC2. The Groth Strip fields (*circles*) and other fields (*crosses*) are shown separately. The vertical line at the left is the color selection criterion $(V-I)_0 \geq 1.07$. The diagonal line is the criterion excluding disk stars within 8 kpc of the Galactic plane and evaluated for $b = 60^\circ$ (appropriate for the Groth Strip). The horizontal line is the approximate magnitude limit for 27 of the 28 Groth Strip fields.

Figure 1 shows this threshold for the Galactic latitude $b = 60^\circ$, the value for the 28 Groth Strip fields. Note that the detected stars are not bunched up against this threshold as they would be if the sample were contaminated by disk stars.

Second, we exclude spheroid turn-off stars and giants by restricting attention to stars with $(V-I)_0 \geq 1.07$. This color cutoff eliminates turn-off stars since these are bluer than the cutoff. Metal-poor giants do exist with $V-I > 1.07$ and

these would remain in the sample if the color inequality were the only selection criterion. However, these metal-poor giants have absolute magnitudes $M_V < 0.6$, which is more than 5.9 mag brighter than disk stars of the same color. Thus, any giant satisfying both criteria would have to lie more than 120 kpc from the Galactic plane, where the density of giants is extremely small. Explicitly, the fraction of giant contaminants in a given apparent-magnitude interval is

$$\frac{N_G}{N_{MS}} = \frac{\nu(D_G, l, b)}{\nu(D_{MS}, l, b)} \left(\frac{D_G}{D_{MS}} \right)^3 \frac{\Phi_G}{\Phi_{MS}} \sim \frac{\Phi_G}{\Phi_{MS}} \quad (2.1)$$

where $\nu(D_G, l, b)$ is the density of giants (relative to their local density) at their distance D_G and Galactic coordinates (l, b) , Φ_G is the local normalization of the giant LF at their absolute magnitude (inferred from their color), and the corresponding quantities for main-sequence stars are similarly defined. The last step follows because both the giants and main-sequence stars are sufficiently far that their Galactocentric distances R are of the same order as their distances from us, D . Since $\nu \sim R^{-3}$, the two terms approximately cancel. Since $\Phi_G/\Phi_{MS} \sim \mathcal{O}(1\%)$, it follows that giant contamination is negligible.

Another potential contaminant is disk white dwarfs. Old white dwarfs could be seen to a distance of 1 kpc and younger WDs could be seen even further. However, using the local disk white dwarf LF of Liebert, Dahn, & Monet (1988) and the vertical disk profile for M dwarfs reported in Paper IV, we find that < 1 WD is expected in the 53 fields combined. White dwarfs should have a vertical profile like the M dwarfs because their main-sequence progenitors have a mixture of ages that is similar to that of M dwarfs.

For completeness, we also consider spheroid white dwarfs. As we show in § 5.1, at the Galactic plane the spheroid has only $\sim 1/600$ of the density of disk. At 1 kpc above the plane, the edge of the volume where the peak of the white dwarf LF is visible, this fraction is $\sim 1/60$. Hence, spheroid white dwarf contamination is almost two orders of magnitude smaller than that caused by disk white dwarfs, and thus completely negligible. Finally, disk giants are far too bright to enter the sample.

QSOs (or AGN of lower luminosity) are another possible source of contamination. The density of QSOs with $B < 22$ is $\sim 200 \text{ deg}^{-2}$ (Hartwick & Schade 1990), implying that a total of ~ 12 QSOs should be present in our fields. While the QSO LF is not known beyond $B = 22$, one might plausibly assume that the number continues to double with each magnitude. Since the survey extends approximately 3 magnitudes beyond this limit, there could be $\mathcal{O}(100)$ such objects in the 53 fields. The great majority of these QSOs are too blue to pass the color selection criterion

of $(V - I)_0 \geq 1.07$. For example, we obtained ground-based V and I photometry of 115 QSOs in the course of measuring the colors of stars found in pre-repair *HST* images (Paper III). Only 7 of these 115 have $(V - I)_0 \geq 1.07$. (These have 1950 coordinates and corresponding redshifts: 0438-43, 2.852; 0846+51, 1.860; 0903+17, 2.771; 1011+09, 2.260; 2121+05, 1.878; 2136+14, 2.427; and 2225-05, 1.981). QSOs should exceed this color limit only if they are at $z > 4$ or have substantial internal extinction. In addition, most AGN are embedded in discernible galaxies. The lower the AGN luminosity, the more likely it is that the diffuse light of the host galaxy will cause the object to be rejected as “non-stellar” in our initial morphological selection. There are no data from which one could measure the rejection fraction precisely, but the one available piece of evidence is encouraging: a $V \sim 25$, $z = 3.368$ emission-line galaxy was identified by two groups in the Hubble Deep Field (HDF) and characterized as “point-source?” by one (Steidel et al. 1996, object C2-11) and “[d]espite some faint extended emission [has the] smallest half-light radius in our sample, $r_{1/2} = 0''.14$, indistinguishable from a point source” by the other (Lowenthal et al. 1997, object hd2_0705_1366). However, in our analysis of HDF (1996, Paper II) we classified this object as “non-stellar” while noting that it is compact.

For the reasons given in the preceding paragraph, we believe that our subdwarf sample is not significantly contaminated by compact extra-galactic objects, and we assume no contamination in the analysis below. This assumption could be tested by searching for QSOs (using either objective-prism or broad-band techniques) in the Large Multi-Color Survey (“Groth Strip”) that comprises 28 of the 53 fields analyzed here. There should be ~ 6 QSOs in these fields with $B < 22$. If these were rejected as “non-stellar” in our morphological selection, it would indicate that contamination is indeed minor. In addition, such a study would provide valuable data on the host environments of faint QSOs that would be complementary to the studies by Bahcall et al. (1997) and Jones et al. (1997) on the hosts of bright QSOs.

We conclude that the sample of 166 spheroid stars is nearly free of contamination. We believe that no more than one, or perhaps a few, members of the sample are objects other than spheroid subdwarfs.

3. Characterization of the Spheroid

3.1. SPHEROID PARAMETERIZATION

We model the distribution of spheroid stars as functions of Galactic coordinates (x, y, z) and absolute magnitude M_V by a flattened power law,

$$n(x, y, z; M_V, c, \ell, R_0) = \Phi(M_V)\nu(x, y, z; c, \ell, R_0), \quad (3.1)$$

where $\Phi(M_V)$ is the local LF, ν is the density of the spheroid as a function of position normalized to the solar neighborhood,

$$\nu(x, y, z; c, \ell, R_0) = \left[\frac{x^2 + y^2 + (z/c)^2}{R_0^2} \right]^{-\ell/2}, \quad (3.2)$$

R_0 is the galactocentric distance, c is the flattening parameter, and ℓ is the power. Thus there are three free galactic-structure parameters (c, ℓ, R_0) , plus one free parameter for each luminosity bin.

3.2. COLOR-MAGNITUDE RELATION

In order to interpret the observables $(I, V - I)$ in terms of the parameters of the model $(\Phi(M_V), c, \ell, R_0)$, one must assume a color-magnitude relation (CMR). For most globular clusters, the main sequence forms a narrow line with very little scatter, and the CMR is a tight one-to-one relation between color and absolute magnitude. By contrast, the spheroid is composed of stars with a wide range of metallicities and thus a range of absolute magnitudes at fixed color. Hence, the one-to-one CMR relation characteristic of globulars must be replaced by a probability distribution. To calibrate this relation, we rely primarily on the CMD of nearby subdwarfs with transverse speeds $V_T > 260 \text{ km s}^{-1}$ kindly provided to us in advance of publication by C. Dahn (1997 private communication). This CMD is updated from the work of DLHG and we therefore refer to it as the “DLHG CMD” or “DLHG stars”. The high velocity DLHG stars should be representative of the stars in our sample, which are found many kpc from the Galactic plane (see below). Unfortunately, the 43 DLHG subdwarfs with $V_T > 260 \text{ km s}^{-1}$ and reliable parallaxes do not sample the CMD densely enough to permit direct construction of a CMR. We therefore use the low-metallicity theoretical isochrones of Baraffe et al. (1997) to interpolate across the DLHG CMD. We proceed as follows: First, we superpose the isochrones (at $[m/H] = -2.0, -1.5, -1.3,$ and -1.0) on the DLHG CMD. We find, as was already noted by Baraffe et al. (1997), that many of the stars are brighter than even the most metal-rich of these isochrones. We therefore

add an additional isochrone at $[m/H] = -0.5$ kindly provided to us by I. Baraffe (1997 private communication). We then estimate the $[m/H]$ of each of the 43 stars by interpolating between the isochrones. We find that the cumulative metallicity distribution, $N([m/H])$, is well represented by $dN/d[m/H] = 0.49$ for $-1.8 < [m/H] < -0.9$, and $dN/d[m/H] = 0.93$ for $-0.9 < [m/H] < -0.3$, with a mean metallicity $\langle [m/H] \rangle = -0.93$. This is somewhat surprising because high-velocity spheroid stars are generally believed to be more metal poor, $\langle [Fe/H] \rangle \sim -1.5$ (Laird et al. 1988; Nissen & Schuster 1991). Part of the difference, perhaps 0.35 dex, can be accounted for by the fact that Population II stars are more deficient in Fe than in metals generally. The remainder could in principle be a result either of a previous error in estimating the mean abundances of spheroid stars or of problems with the theoretical isochrones. Gizis (1997) measured the metallicities of a subset of the high-velocity DLHG stars and found that they lay in the traditional normal range for metal-poor stars, $[Fe/H] \sim -1.5$. He noted, as we have, that the Baraffe et al. (1997) isochrones appear to be inconsistent with this metallicity and pointed out that the previous generation of the same code (Baraffe et al. 1995) seemed to yield closer agreement with his spectroscopically measured metallicities. On the other hand, I. Baraffe (1998, private communication) and her collaborators believe that the new codes are superior in that they take account of more of the physics and show better agreement with globular-cluster data. Thus, the issue remains unresolved. Fortunately, for present purposes, the discrepancy is not a concern because we use the theoretical isochrones only to interpolate between the data points. However, as we discuss below, this discrepancy will be of greater concern when we estimate the subdwarf MF.

3.3. KINEMATIC VERSUS PHOTOMETRIC SELECTION

The DLHG stars were selected according to kinematic criteria and therefore could in principle be biased relative to the photometrically selected *HST* sample. Suppose that the spheroid were composed of sub-populations and that those populations with a larger asymmetric drift relative to the Local Standard of Rest, v_a , also had lower metallicities. The DLHG sample that we use to calibrate the CMR is selected from stars with transverse velocity $V_T > 260 \text{ km s}^{-1}$, so the stars with lower metallicity would be over-represented. Since these are more subluminous, we would tend to underestimate the luminosities and hence the distances of the stars in our sample. We now argue that this bias is likely to be small on the basis of two complementary arguments.

First, two independent estimates of local spheroid kinematics find very similar results. Casertano, Ratnatunga, & Bahcall (1990, hereafter CRB) find dispersions $(\sigma_R, \sigma_\phi, \sigma_z) = (160, 89, 94) \text{ km s}^{-1}$ and $v_a = 217 \text{ km s}^{-1}$ from samples of high

proper motion stars. Layden et al. (1996) find $(\sigma_R, \sigma_\phi, \sigma_z) = (168, 102, 97) \text{ km s}^{-1}$ and $v_a = 198 \text{ km s}^{-1}$ using spheroid RR Lyrae stars whose selection depends only weakly on kinematic criteria. The spheroid is therefore rotating very slowly. If the spheroid is composed of subpopulations, each subpopulation is probably also rotating slowly. Otherwise, some subpopulations would have to be counter-rotating. The difference in bulk velocity between populations should then be no more than a few tens of km s^{-1} . We find numerically that the selection function for the DLHG stars for $v_a = 230 \text{ km s}^{-1}$ is only $\sim 30\%$ higher than for $v_a = 200 \text{ km s}^{-1}$. Even if the entire dispersion in the DLHG CMD of $\sigma \sim 0.4 \text{ mag}$ is due to metallicity variation that is perfectly correlated with asymmetric drift, this implies that the bias toward underestimating the luminosity of the stars in our sample is only $\sim 0.1 \text{ mag}$.

Second, Beers & Sommer-Larson (1995) have used radial velocities to measure the asymmetric drift of a non-kinematically selected sample of metal-poor stars as a function of metallicity. They find that for $[\text{Fe}/\text{H}] < -1.5$, the asymmetric drift is constant (see their Fig. 6). For more metal-rich stars, there is a strong dependence on metallicity. Chiba & Yoshii (1998) find a similar result from a sample of metal-poor giants and RR Lyrae stars with Hipparcos proper motions (see their Fig. 5). The simplest interpretation of these results is that the stars with $[\text{Fe}/\text{H}] < -1.5$ are drawn almost entirely from the spheroid, and that the spheroid has no differential rotation. The more metal-rich parts of this sample are increasingly contaminated with disk or thick disk stars. In brief, we believe that we and DLHG are sampling essentially the same population.

4. Analysis

4.1. PROPERTIES OF THE SAMPLE

Figure 2 shows the approximate positions (*crosses*) of the 166 stars in cylindrical coordinates (ρ, z) where $\rho^2 \equiv x^2 + y^2$. The distances are determined from the measured colors and apparent magnitudes, and assuming the color-magnitude relation for the $[\text{m}/\text{H}] = -1.0$ isochrone of Baraffe et al. (1997). Also shown is the minimum distance from the plane (2.34 kpc) that spheroid stars could have been detected due to the exclusion of disk stars within 8 kpc of the Galactic plane (*solid lines*). The apparent discrepancy between these two distances is due to the fact that spheroid stars can be as much as $5 \log(8/2.34) = 2.67 \text{ mag}$ fainter than disk stars at the same color. The maximum distances probed for each of the 53 fields are shown as (*circles*). Note that these circles *do not* represent detected stars. The densely populated “plume” is the Groth Strip.

Note that the spheroid is well sampled in several substantially different directions out to Galactocentric distances of $R \sim 20 \text{ kpc}$ and that most lines of sight

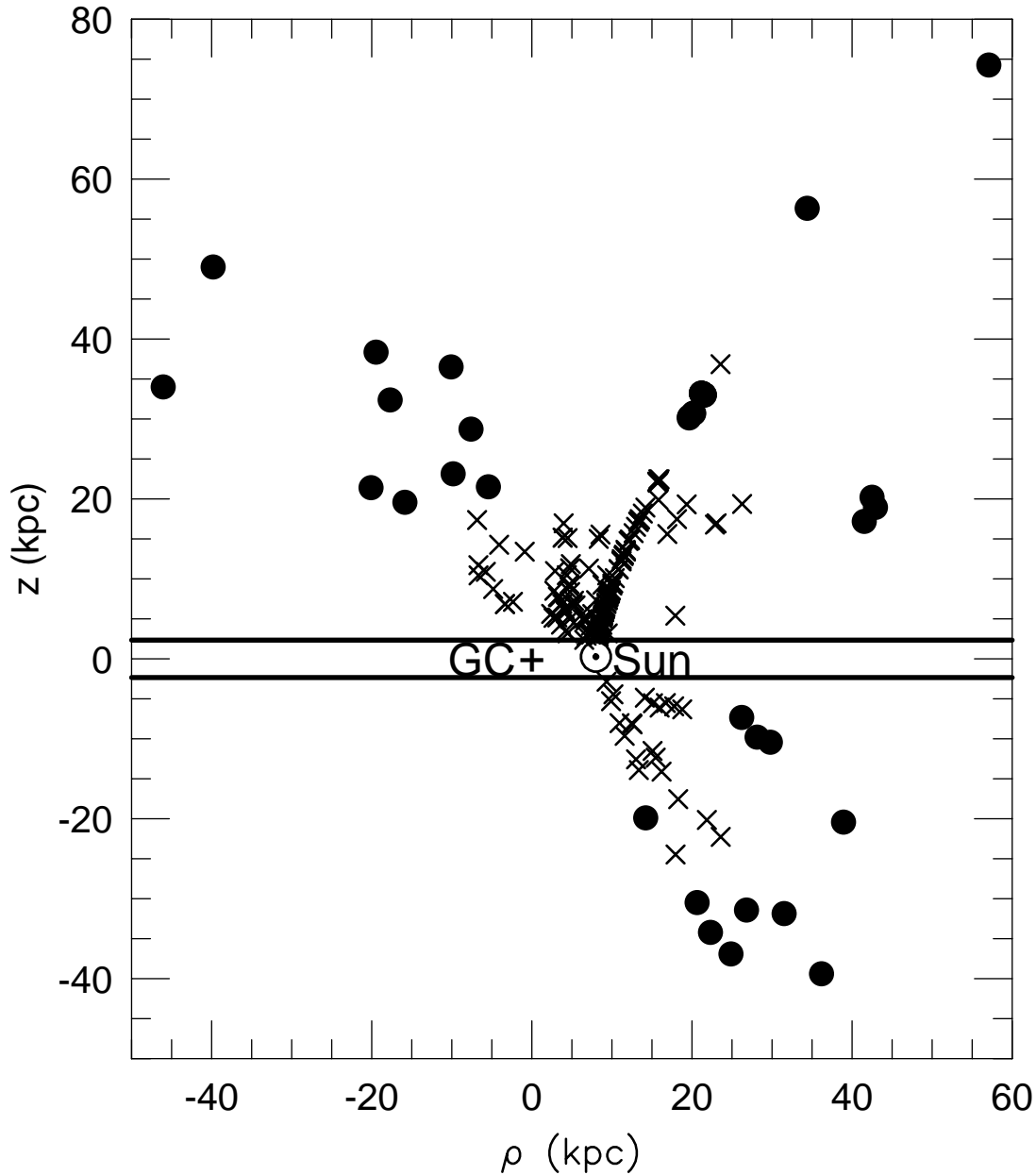


Figure 2. Galactic coordinates (ρ, z) of 166 spheroid stars (*crosses*) found in 53 *HST* WFC2 fields, together with the most distant coordinates probed by each field (*circles*). Note that the circles *do not* represent detected stars. Here $\rho^2 = x^2 + y^2$ and ρ is defined to have the same sign as x . The Galactic center is shown as a “+” and the Sun’s position is shown as a “⊙”. The two horizontal lines (at $z = \pm 2.34$ kpc) represent the exclusion of disk stars within 8 kpc of the Galactic Plane. The apparent discrepancy between these two distances arises because spheroid stars can be as much as $5 \log(8/2.34) = 2.67$ mag fainter than disk stars at the same color. All distances are evaluated using the $[m/H] = -1.0$ isochrone of Baraffe et al. (1997). The dense “plume” is the Groth Strip.

probe to $R \sim 40$ kpc (even though there are relatively few detections at these large distances). These characteristics give good leverage on the Galactic structure flattening parameter, c and the power law, ℓ . The fact that some lines of sight

extend to negative x values (shown as negative ρ in Fig. 2) implies that the sample should give modest leverage on R_0 . Note that the most distant star detected has a galactocentric distance $R \sim 45$ kpc.

4.2. LIKELIHOOD FUNCTION

Let τ_{ijk} be the expected number of stars in the bin of apparent magnitude I_i , color $(V - I)_j$, for the k th field. The Poisson probability of finding n_{ijk} stars in this bin is then $P_{ijk} = \exp(-\tau)\tau^n/n!$. If the bins are chosen to be very small so that $\tau \ll 1$, then $n = 0$ or $n = 1$, so $n! \rightarrow 1$. Hence, the logarithm of the likelihood is

$$\ln L = \sum_{i,j,k} \ln P_{ijk} = \sum_{i,j,k} n_{ijk} \ln(\tau_{ijk}) - \sum_{i,j,k} \tau_{ijk}. \quad (4.1)$$

The second term on the right hand side is simply N_{exp} , the expected total number of stars to be detected for the model, while the first reduces to a sum over the detected stars:

$$\ln L = \sum_{\text{det},i,j,k} \ln \tau_{ijk} - N_{\text{exp}}. \quad (4.2)$$

To maximize $\ln L$ over the class of models represented by equation (3.1), we need to predict τ_{ijk} as a function of Galactic parameters. We first evaluate $\text{CMD}_{i'j'l}$, the color-magnitude distribution in M_I and $(V - I)_0$ (binned by indices i' and j') of stars uniformly distributed over the l th bin of absolute magnitude M_V , and distributed in metallicity as described in § 3.2. For each distance-modulus bin μ_m , we then construct a normalized color-apparent magnitude diagram cmd_{ijklm} by first translating $\text{CMD}_{i'j'l}$ by $\mu_m + A_{I,k}$ in the magnitude direction and $E_k(V - I)$ in the color direction, and then convolving with the observational errors. We define the local volume element

$$V_{k,m} = \frac{\ln 10}{5} 10^{0.6\mu_m+3} \Omega_k \Delta\mu \text{ pc}^3, \quad (4.3)$$

where Ω_k is the angular area of the k th field (see Paper IV) and $\Delta\mu$ is the width of the distance modulus bins. This allows us to write the first term in equation (4.2) as

$$\sum_{\text{det},i,j,k} \ln \tau_{ijk} = \sum_{n=1}^{N_{\text{det}}} \ln \sum_{l,m} \Phi_l \nu_{k(n),m}(c, \ell, R_0) V_{k(n),m} \text{cmd}_{i(n),j(n),k(n),lm}, \quad (4.4)$$

where N_{det} is the total number of stars detected in all fields, and ν is the Galactic structure function given by equation (3.1). We adopt bin sizes of 0.1 mag for the

magnitude indices over which we integrate (i, i' , and m) and 0.025 magnitudes for the color indices (j and j'). Similarly, we write the second term in equation (4.2) as

$$N_{\text{exp}} = \sum_{k,l,m} \Phi_l \nu_{km}(c, \ell, R_0) V_{km} \text{cmd}_{\text{tot},klm}, \quad (4.5)$$

where

$$\text{cmd}_{\text{tot},klm} \equiv \sum_{\text{selection},i,j} \text{cmd}_{ijklm}, \quad (4.6)$$

and where the sum is restricted to the portions of the CMD satisfying the selection criteria. The matrices $\text{cmd}_{i(n),j(n),k(n),lm}$ and $\text{cmd}_{\text{tot},klm}$ can be evaluated in about 15 minutes on a SPARC 5. Once these are determined, the likelihood function and its derivatives with respect to all the parameters can be evaluated in about 1 second, and hence parameter space can be explored rapidly.

4.3. LUMINOSITY FUNCTION

4.3.1 Best-Fit LF

We use the formalism of the previous section to evaluate simultaneously the Galactic structure parameters c, ℓ , and R_0 and the LF with the latter being broken up into four 2-mag bins centered at $M_V = 7.5, 9.5, 11.5$, and 13.5 . We note that the full range of the LF must be chosen broad enough so that no stars in the detected color range $1.07 \leq (V - I)_0 \leq 2.52$ could have absolute magnitudes outside the range of the LF. Otherwise, any such stars that are detected will be falsely attributed by the likelihood function to stars within the range, and the LF will be overestimated. The adopted limits satisfy this criterion. On the other hand, there is no systematic tendency to underestimate the LF if the end bins extend somewhat beyond the color-selection range, since the likelihood function automatically takes this selection into account. We find

$$c = 0.96 \pm 0.22, \quad \ell = 2.96 \pm 0.27, \quad R_0 = 6.2 \pm 1.8 \text{ kpc}, \quad (4.7)$$

and LF (in units of 10^{-5} pc^{-3}) $\Phi(7.5) = 1.05 \pm 0.55$, $\Phi(9.5) = 1.37 \pm 0.64$, $\Phi(11.5) = 1.98 \pm 0.78$, and $\Phi(13.5) = 1.64 \pm 1.20$. While it is encouraging that the solution for R_0 in equation (4.7) is consistent with other determinations, our error bars are not competitive with other methods of measuring the galactocentric distance. We henceforth fix $R_0 = 8 \text{ kpc}$ (Reid 1993) in all further calculations. We then find

$$c = 0.82 \pm 0.13, \quad \ell = 3.13 \pm 0.23, \quad (R_0 \equiv 8.0 \text{ kpc}) \quad (4.8)$$

and a LF which is similar in shape to the one obtained without fixing R_0 , but is

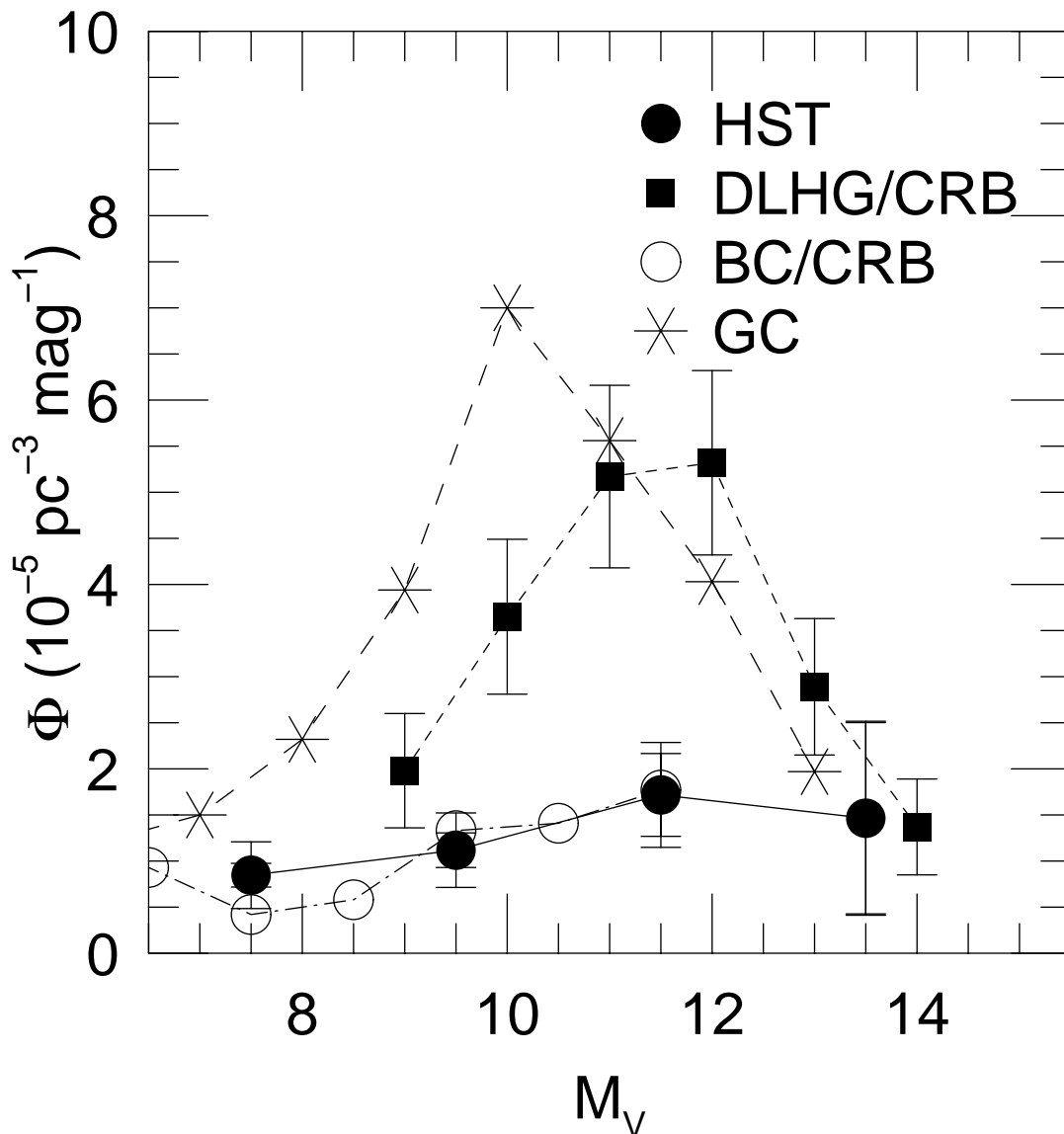


Figure 3. Luminosity functions of the spheroid as determined in this paper using *HST* data (*filled circles*) compared to that of DLHG (*squares*) and BC (*open circles*). Also shown is the average LF of three metal-poor globular clusters (*stars*) as measured by Piotto et al. (1997). The DHLG and BC LFs have been multiplied by 0.75 and 0.62 respectively based on a reanalysis of spheroid kinematics by CRB. The globular cluster LF is normalized arbitrarily. Two sets of error bars are shown for the *HST* LF. The smaller errors assume that the Galactic structure parameters are fixed. The pattern of these error bars shows that the LF of brighter stars is much more sensitive to assumptions about Galactic structure compared to the LF of fainter stars. To avoid clutter, no error bars are shown for the BC LF. In addition, the last point of the BC LF (at $M_V = 12.5$) is not shown because it is based on only two stars.

about 15% smaller in normalization: $\Phi(7.5) = 0.85 \pm 0.36$, $\Phi(9.5) = 1.12 \pm 0.40$, $\Phi(11.5) = 1.72 \pm 0.57$, and $\Phi(13.5) = 1.46 \pm 1.05$.

Figure 3 shows the LF derived in this paper along with the local spheroid LFs of DLHG and BC and an average LF of three metal-poor globular clusters (NGC 6341, NGC 7078, and NGC 7099) measured by Piotto, Cool, & King (1997). The DLHG and BC LFs are multiplied by a factor 0.75 and 0.62 respectively (as discussed below), and the cluster LF is arbitrarily normalized.

The *HST* spheroid LF is shown with two sets of error bars. One set of errors is obtained as described above. The other (smaller) error bars are determined by fixing the Galactic structure parameters c and ℓ at their best-fitting values. Note that the difference is dramatic for the brightest bin but noticeable only with a magnifying glass for the faintest bin. This is because the brighter stars probe distant regions of the Galaxy and hence their LF is highly correlated with the Galactic structure parameters. By contrast, the fainter stars are relatively nearby and hence insensitive to assumptions about the large-scale structure of the Galaxy. Another feature of the *HST* LF, which is not illustrated in Figure 3, is that the individual luminosity bins are anti-correlated with one another. When c and ℓ are held fixed, neighboring bins have correlation coefficients of about -0.3 . This is due to the fact that most detected stars can be almost equally well attributed to either of two neighboring luminosity bins. These various correlations among the parameters make the interpretation of Figure 3 less straight forward than one would like.

The major question posed by Figure 3 is: are the DLHG and *HST* LFs consistent? Before addressing this question, we first justify our reduction of the DLHG and BC LFs by a factor of 0.75 and 0.62 respectively.

4.3.2 Spheroid Kinematics and the DLHG and BC LFs

BC selected stars with transverse speeds $V_T > 220 \text{ km s}^{-1}$ and assumed that the underlying spheroid population had characteristics given by their two component Galactic model, namely $v_a = -154 \text{ km s}^{-1}$ and $(\sigma_R, \sigma_\phi, \sigma_z) = (140, 100, 76) \text{ km s}^{-1}$. Based on this model, they calculated that a fraction 0.33 of spheroid stars satisfied their transverse-speed selection criterion. Subsequently, CRB showed that a significantly better fit to the same data can be obtained by assuming that there is a third population with intermediate kinematics. The spheroid component is then moving much more rapidly relative to the Sun: $v_a = -217 \text{ km s}^{-1}$, $(\sigma_R, \sigma_\phi, \sigma_z) = (160, 89, 94) \text{ km s}^{-1}$ (CRB). As we discussed in § 3.1, this determination is in excellent agreement with the kinematics of spheroid RR Lyrae stars as measured by Layden et al. (1996). We have therefore redone the calculation using BRC kinematics and find a completeness factor 0.54. Hence we multiply the BC results by a factor $0.33/0.54 = 0.62$ and label the modified BC LF as “BC/CRB”. DLHG also selected stars with transverse speeds $V_T > 220 \text{ km s}^{-1}$. They used slightly different kinematic assumptions and derived a completeness fac-

tor of $1/2.46$. We therefore multiply their results by a factor $1/(2.46 \times 0.54) = 0.75$ and label the resulting LF “DLHG/CRB”.

4.3.3 Comparison of the *HST* and DLHG/CRB LFs

From Figure 3, one sees that the DLHG/CRB LF is overall higher than the *HST* LF, particularly near the peak of the former, $M_V \sim 11.5$. However, as we emphasized above, the correlations among the parameters render difficult the interpretation of the figure. The appropriate method to determine whether these two measurements are consistent is to fix the *HST* LF at the DLHG/CRB values for the three overlapping bins ($M_V = 9.5, 11.5,$ and 13.5) and to allow the other parameters to vary. We find that the best-fit such solution has an increase in χ^2 (i.e. $-2 \ln L$), of 11.4 for three more degrees of freedom. This means that the two LFs differ at the 2.9σ level. We note for completeness that this solution yields $c = 0.638 \pm 0.050$ and $\ell = 3.27 \pm 0.22$. Of course, one might also solve for the LF that minimizes χ^2 for the two samples simultaneously, rather than imposing the DLHG/CRB solution of the *HST* data. However, we find that the best-fit such solution is still discrepant by 2.8σ .

The LFs of the spheroid and the globular clusters cannot be directly compared because they are of different metallicities. We reserve comparison for our discussion of MFs.

4.3.4 Possible Explanations for the Discrepancy Between LFs

One possible reason for the discrepancy between between the *HST* and DLHG/CRB LFs is a statistical fluctuation. Assuming Gaussian statistics, the chance of a 2.8σ event is $\sim 0.5\%$, but the probability would rise rapidly if even a modest part of the difference between the LFs were due to unrecognized systematic errors in either determination. One indication of the possible size of such systematic errors is the conflict between the DLHG/CRB LF and the BC/CRB LF, both of which were based on local proper-motion selected samples. As we discussed in § 1, the most likely cause of this conflict is that the BC LF is based on Eggen’s (1979b) linear, single-valued CMR while the DLHG LF is based on trigonometric parallaxes. Hence, the DLHG solution is to be preferred a priori over that of BC. Nevertheless, it is striking that the BC/CRB LF is actually in very good agreement with the *HST* LF. In brief, we believe that no strong conclusions can be drawn from the apparent conflict between the *HST* and DLHG/CRB LFs.

Just the same, it is worth asking if this difference could be a real effect. Sommer-Larsen & Zhen (1990) have proposed that the spheroid has two components, a highly flattened component which contributes about 40% of the total density in the neighborhood of the Sun, and a nearly spherical component ($c = 0.85 \pm 0.12$) which contributes the other 60%. We emphasize that the

model’s flattened component is supported by an anisotropic velocity dispersion tensor, in contrast to the more traditional (and also highly flattened) intermediate or “thick disk” population which is supported by rotation. Sommer-Larsen & Zhen (1990) developed this model based on 118 non-kinematically selected stars with $[\text{Fe}/\text{H}] \leq -1.5$. Hartwick (1987) advanced a similar notion on the basis of a study of RR Lyrae stars with $[\text{Fe}/\text{H}] \leq -1.0$, but this sample is almost certainly contaminated with intermediate population stars.

If the Sommer-Larsen & Zhen (1990) model were correct, then only the spheroidal component would enter the *HST* sample. The flattened component would be effectively eliminated because the selection criteria remove all stars within several kpc of the plane (see Fig. 2). It would then be appropriate to multiply the DLHG/CRB LF by 0.6 before comparing it to the *HST* LF. We find that χ^2 then rises by only 3.6 for three more degrees of freedom. That is, the two LFs are consistent at the 1σ level. Thus, the discrepancy between the *HST* and DLHG/CRB LFs could plausibly be explained by a two-component spheroid. However, we caution that the evidence for a two-component spheroid is limited, and it is quite possible that the discrepancy is due to a combination of systematic and statistical errors.

We note that a prediction of the two-component model is that the velocities of spheroid stars perpendicular to the plane should contain a hot and cold component, and therefore the velocity distribution should have a kurtosis in excess of the Gaussian value $K = 3$. Popowski & Gould (1998) find $K = 4.5$ for 165 “halo-3” RR Lyrae stars. For present purposes, it is more appropriate to use the subsample of 97 stars restricted to $[\text{Fe}/\text{H}] < -1.5$. For these we find $K = 4.7$. This is inconsistent with the Gaussian value at the 2.7σ level.

4.4. MASS FUNCTION

It is customary to determine the MF of a stellar population by first measuring its LF and then converting to a MF using a mass-luminosity relationship. However, the spheroid is composed of stars with a wide range of metallicities and hence a correspondingly wide range of masses at fixed luminosity; thus the usual procedure for determining a MF is not applicable. Moreover, the observables for our spheroid sample are color and flux (not luminosity) and there is no one-to-one relation between color and flux and either luminosity or mass.

We adopt a different approach which is similar to the LF measurement that we described in § 4. We repeat for the mass function all the steps described in § 4 except that we initially construct $\text{CMD}_{i,j,l}$ with l running over *mass bins*, M_l , rather than absolute magnitude bins as before. That is, we draw stars uniformly in log mass rather than log luminosity. We use exactly the same models from Baraffe et al. (1997) to do this with exactly the same metallicity distribution. We

stress that while this substitution is mathematically and computationally easy to perform, it contains strong additional assumptions relative to the LF case. For the LF, the Baraffe et al. (1997) isochrones served only as interpolators between the DLHG data points. As such, systematic errors in the isochrones would most probably not propagate into the analysis. By contrast, the “mass” in these models is a purely theoretical quantity with no empirical calibration. That is, the situation is very different than for the disk MF (Paper IV) where an excellent empirical mass-luminosity relation exists (Henry & McCarthy 1993). Thus, the determination of the spheroid MF is on fundamentally weaker ground compared to the spheroid LF.

We use the procedure just described to evaluate the MF over the range $0.09 < M/M_\odot < 0.71$, the limits being established according to the criterion outlined at the beginning of § 4.3.1. For four mass bins centered at $(M/M_\odot) = 0.55, 0.33, 0.20,$ and 0.12 , we find $dN/d\log M = 14 \pm 6, 6 \pm 4, 12 \pm 10,$ and 19 ± 14 in units of 10^{-5}pc^{-3} . The Galactic structure parameters are $c = 0.80 \pm 0.12$ and $\ell = 3.15 \pm 0.23$, i.e., almost identical to the values in the LF solution (eq. (4.8)). This MF shows some hint of structure with a dip in the second bin, but one may suspect that (as in the LF case) there is not actually enough information in the data to resolve this structure.

To test the information content of the data, we fit them directly to a power-law mass function of the form

$$\frac{dN}{d\log M} = G(M; A, \alpha) = A \left(\frac{M}{M_\odot} \right)^\alpha. \quad (4.9)$$

We modify the likelihood analysis discussed above in two ways. First, we calculate cmd_{ijklm} for a large number of mass bins M_l (in practice, $l = 1, \dots, 16$). Second, we write N_{exp} as

$$N_{\text{exp}}(c, \ell, R_0, A, \alpha) = \sum_{k,l,m} G(M_l; A, \alpha) \nu_{km}(c, \ell, R_0) V_{km} \text{cmd}_{\text{tot},klm} \Delta \log M, \quad (4.10)$$

where $\Delta \log M$ is the width of the logarithmic mass bin. We also write an analogous expression for the first term in equation (4.2). We find

$$c = 0.79 \pm 0.12, \quad \ell = 3.06 \pm 0.22, \quad (MF), \quad (4.11)$$

and MF parameters $A = 13.5 \pm 7.4 \times 10^{-5} \text{pc}^{-3}$ and $\alpha = 0.25 \pm 0.32$. The error in the MF normalization, A , appears to be extremely large but this is because the mass normalization (M_\odot) lies outside the range of the data. Hence, A and α are

highly correlated. The correlation can be eliminated by normalizing to $0.225 M_{\odot}$:

$$\frac{dN}{d \log M} = (9.4 \pm 2.6) \times 10^{-5} \left(\frac{M}{0.225 M_{\odot}} \right)^{0.25 \pm 0.32} \text{pc}^{-3}. \quad (4.12)$$

The χ^2 is 4.5 higher for the power-law solution compared to the previous 4-bin solution, with 2 more degrees of freedom. The binned solution is therefore favored at the 1.6σ level, which could be due to a statistical fluctuation, systematic errors, or real structure in the MF. In the absence any compelling evidence for structure, we adopt the simpler power-law parameterization given by equation (4.12) as our best estimate of the MF.

5. Discussion

5.1. COMPARISON OF GALACTIC STRUCTURE PARAMETERS

The best-fit Galactic-structure parameters in the LF and MF fits are similar, ($c = 0.79 \pm 0.12$, $\ell = 3.06 \pm 0.22$) and ($c = 0.82 \pm 0.13$, $\ell = 3.13 \pm 0.23$), respectively. These may be compared to previous determinations by various methods.

Kinman, Wirtanen, & Janes (1965) were the first to measure the spheroid flattening. They obtained $c = 0.57$ from RR Lyrae stars. Bahcall (1986) found $c = 0.80^{+0.20}_{-0.05}$ based on star counts. Gilmore (1989) found c to vary with Galactocentric radius, with $c \sim 0.5$ in the solar neighborhood, also based on star counts. Most recently, Preston, Schectman, & Beers (1991) also found c to vary with Galactocentric radius, but with $c \sim 0.7$ in the solar neighborhood from RR Lyrae stars.

Preston et al. (1991) measured the power-law $\ell = 3.2 \pm 0.1$ for RR Lyrae stars, and $\ell \sim 3.5$ for blue horizontal branch stars, the latter being less well determined. They noted that these values were in good agreement with the value $\ell = 3.5$ measured by both Harris (1976) and Zinn (1985) for globular clusters.

Thus, the best-fit power-law found here is consistent with that of RR Lyrae and blue horizontal branch stars. The flattening is consistent with the recent determination from RR Lyrae stars and with Bahcall's (1986) measurement from star counts. It is in conflict with Gilmore's (1989) determination at about the 2.5σ level.

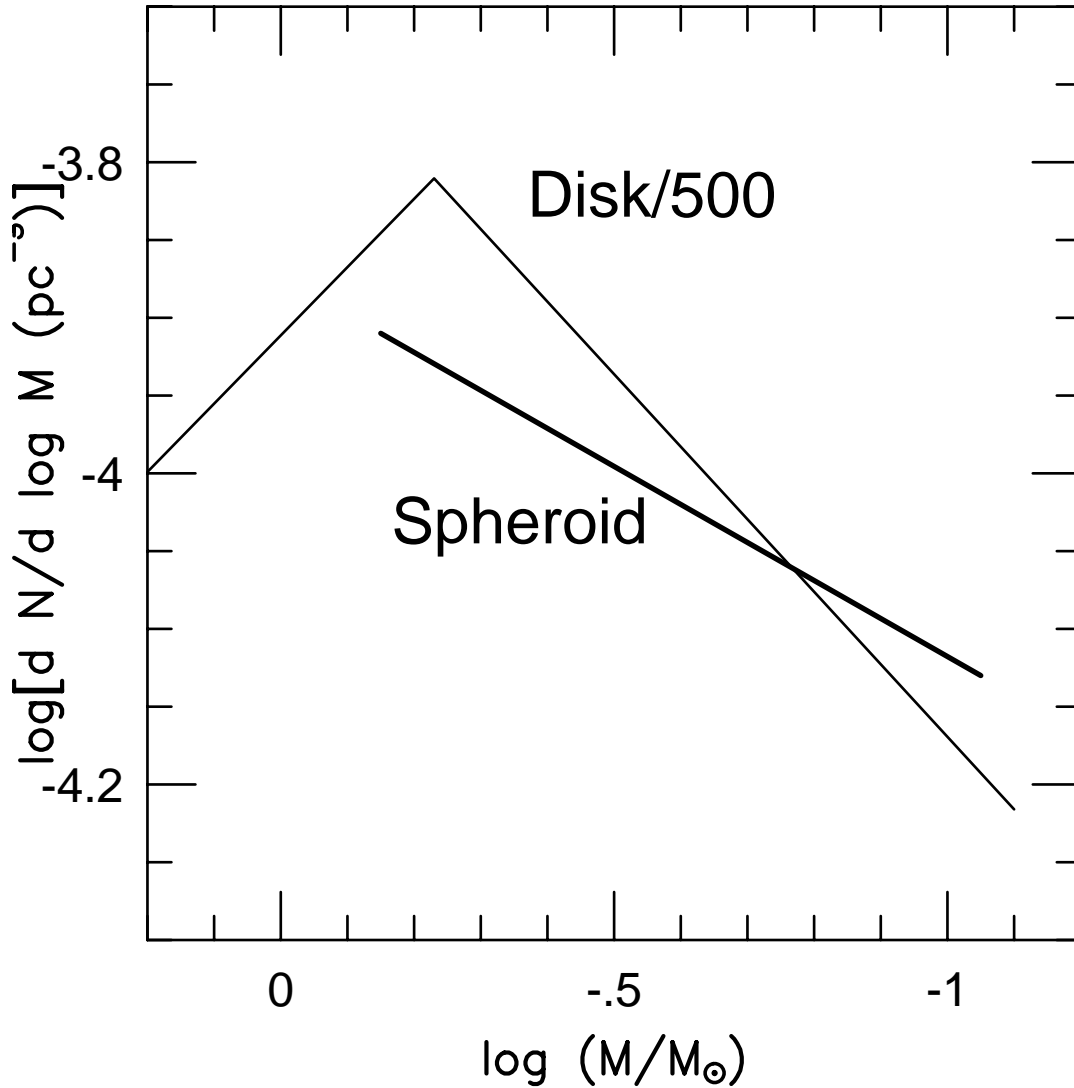


Figure 4. MF for the spheroid (*bold line*) and the disk (*solid line*) as derived in this paper and Paper IV based on *HST* WFC2 data. The disk MF has been divided by 500.

5.2. COMPARISON OF MASS FUNCTIONS

Figure 4 compares the disk MF derived in Paper IV with the spheroid MF derived here. Neither is corrected for binaries. In Paper IV, we argued that binaries should decrease the exponent of (i.e., “steepen”) the disk MF by ~ 0.35 for $M < 0.6 M_{\odot}$, and so make the right-hand part of the solid curve in Figure 4 almost flat. We also argued that the correction for binaries should not affect the slope at the high-mass end. To our knowledge, there are no data on the fraction of spheroid M stars in binary systems and so we prefer to report the uncorrected result. However, it may be plausible to assume a similar correction for the disk and

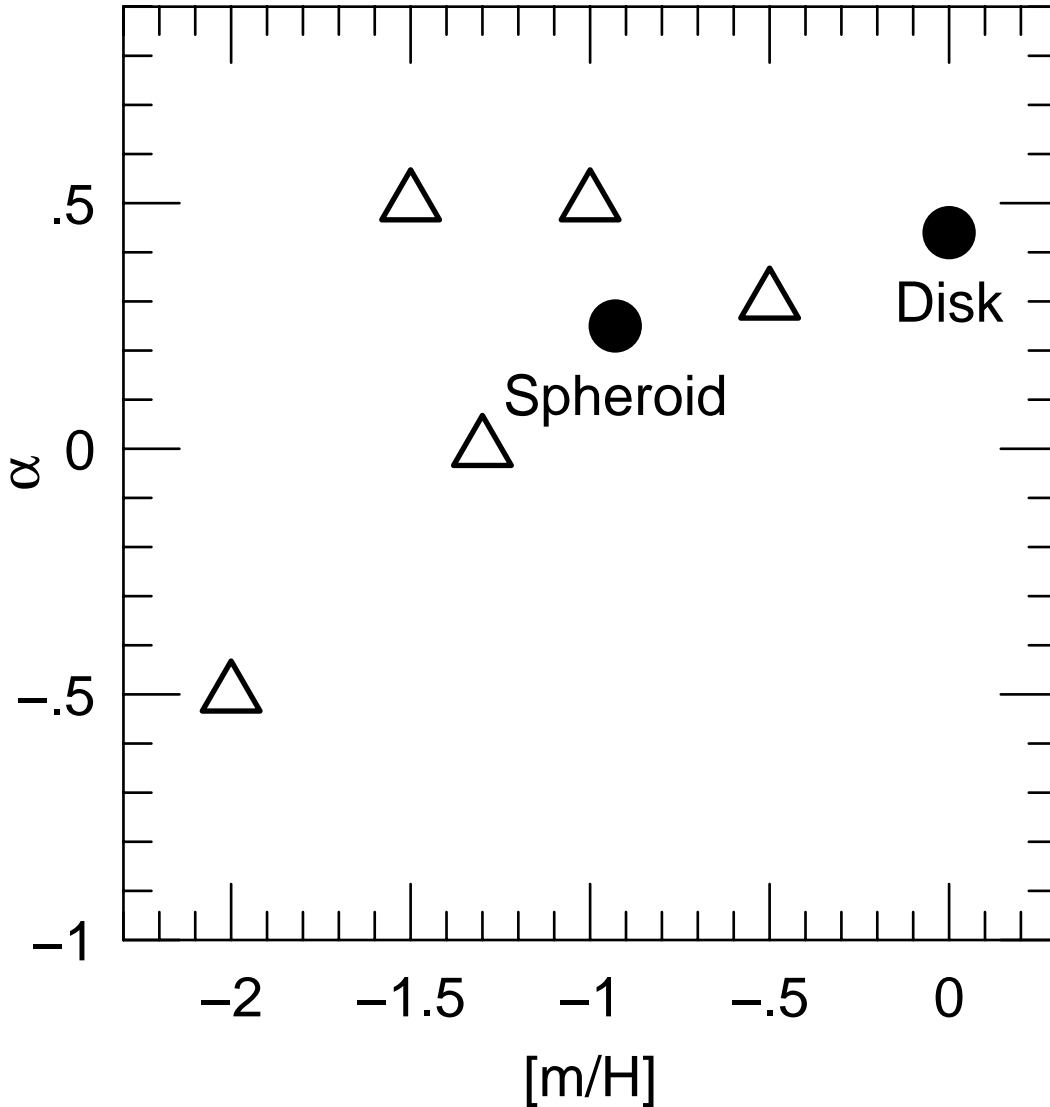


Figure 5. Power-law index (α) versus metallicity ($[m/H]$) for the disk and spheroid (*circles*) as determined from *HST* data and for five groups of globular clusters (*triangles*) as determined by Chabrier & Méra (1997).

spheroid, in which case the spheroid MF would also be approximately flat. The uncorrected spheroid and disk MFs have similar slopes and differ in normalization by a factor 570 ± 160 at the centroid of the spheroid determination, $M = 0.225 M_{\odot}$.

In addition to comparing the spheroid MF to that of the disk, it is of interest to compare it to the MF of other metal-poor systems, specifically globular clusters. Capaccioli, Piotto, & Stiavelli (1993) have analyzed the MF slopes of 17 globular clusters over the range $0.5 M_{\odot} \leq M \leq 0.8 M_{\odot}$. The slopes span a range $-1.2 \lesssim \alpha \lesssim 1$ and show clear trends with galactocentric radius and distance from the plane.

Capaccioli et al. (1993) argue that this pattern confirms the prediction of Stiavelli et al. (1991) that all clusters begin their life with the same MF (i.e., $\alpha \sim -1.2$) and the clusters subject to the greatest dynamical effects preferentially lose their low mass stars. Since the spheroid MF is not affected by dynamics, one would expect its MF to also have this slope, assuming the spheroid and globular cluster MFs are similar. This expectation is in strong conflict with our result, $\alpha = 0.25 \pm 0.32$. However, it is possible that the slope of the spheroid MF changes significantly at $M \sim 0.6 M_{\odot}$ just as we have argued it does for the disk (Paper IV), in which case the two MFs might still be consistent. Capaccioli et al. (1993) also analyzed some cluster MFs over the mass range $M \leq 0.4 M_{\odot}$ but regarded the mass-luminosity relations upon which they based their analysis as unreliable.

Chabrier & Méra (1997) have measured the MF of several globular clusters by applying the Baraffe et al. (1997) isochrones (used to derive our spheroid MF in § 4) to LFs from five groups of globular clusters. While the mass range varies from cluster to cluster, it extends close to the bottom of the main sequence for most. The most metal-poor of these groups ($[m/H] \sim -2.0$) is NGC 6341, NGC 7078, and NGC 7099, the same group whose LF is displayed in Figure 3. The most metal rich is 47 Tuc at $[m/H] \sim -0.5$. The metallicities $[m/H]$ and slopes α of the five groups are displayed in Figure 5 as triangles. The slopes of the spheroid MF (§ 4.4) and of the disk MF (Paper IV) are shown as solid circles. None of the determinations are corrected for binaries. The slopes of the disk and spheroid MFs are consistent with the range set by the globular clusters of intermediate to higher metallicities. Only the three extreme low-metallicity clusters at $[m/H] \sim -2.0$ have a slope substantially below (steeper than) this range. There is still controversy about the evaluation of globular cluster MFs. In particular, Piotto et al. (1997) find $\alpha \sim -1$ for the three most metal-poor clusters compared to the value $\alpha = -0.5$ found by Chabrier & Méra (1997).

5.3. MASS DENSITY OF THE SPHEROID

In order to make a realistic estimate of the mass density of the spheroid, one must account for not only the detected objects ($0.09 < M/M_{\odot} < 0.71$) but also those that for one reason or another escape detection. The latter include substellar objects ($M < 0.09 M_{\odot}$), upper main-sequence stars and evolved stars ($0.71 < M/M_{\odot} \lesssim 0.9$), remnants (which have progenitor masses $M \gtrsim 0.9 M_{\odot}$), and binary companions of the detected stars. In order to isolate the uncertainties due to the last, we perform the entire calculation twice, first accepting equation (4.12) at face value and then correcting it for missing binaries.

There are essentially no empirical data on substellar objects and very little on higher-mass stars and remnants in the spheroid. We therefore make our estimates

based on plausible, if highly debatable, assumptions. For substellar objects, we assume that the power-law observed in the stellar-mass range continues into the brown dwarf regime to zero mass. For the higher-mass stars and progenitors of remnants we assume a break in the power-law to $\alpha = -1.7$ at the upper boundary of the observations, that is,

$$\frac{dN}{d\log M} = 12.5 \times 10^{-5} \left(\frac{M}{0.71 M_{\odot}} \right)^{-1.7} \text{pc}^{-3} \quad (M > 0.71 M_{\odot}). \quad (5.1)$$

We now justify this somewhat arbitrary estimate. There are only limited data constraining the slope of the MF of metal-poor populations in the regime $M > 0.71 M_{\odot}$. BC have measured the LF of spheroid turn-off stars ($0.7 \lesssim M/M_{\odot} \lesssim 0.9$). They find (in units of 10^{-5}pc^{-3} and after the correction discussed in § 3.2) of $\Phi(4.5) = 0.12 \pm 0.12$, $\Phi(5.5) = 0.29 \pm 0.14$, $\Phi(6.5) = 0.93 \pm 0.24$, and $\Phi(7.5) = 0.42 \pm 0.10$. For comparison, we found $\Phi(7.5) = 0.85 \pm 0.36$ in § 4.3 (see Fig. 3). In principle, it would be possible to convert this LF to a MF and measure the slope. In practice, the shortness of the baseline ($\Delta \log M \sim 0.1$) and the size of the statistical errors make this impossible. An alternative approach would be to extend the log-mass baseline by measuring the LF of spheroid white dwarfs. By combining this LF with white-dwarf cooling theory, one could hope to reconstruct the MF of the white dwarf progenitors. In fact, the white dwarf sample of Liebert et al. (1988) contains only 4 stars with transverse velocities $V_T > 200 \text{ km s}^{-1}$. These have $M_V = 13.4, 13.6, 14.3, \text{ and } 15.4$, and so have progenitors of mass $M \sim M_{\odot}$. Hence, the baseline is again too short and the statistical fluctuations too large to determine the slope.

Another approach would be to adopt the MF measured for the upper main sequence of globular clusters. Recall from § 5.2 that Capaccioli et al. (1993) measured a wide range of slopes for a collection of 17 clusters in the mass interval $0.5 M_{\odot} \leq M \leq 0.8 M_{\odot}$, but argued that this variation was an artifact of dynamical effects. They concluded that the initial MF (the quantity most relevant to the spheroid MF which does not suffer dynamical effects) is universal with $\alpha \sim -1.2$. In fact, our adopted equation (5.1) has a similar slope. However, the main problem with all of these empirical estimates of Population II MFs is that they apply only to a narrow range of masses below $1 M_{\odot}$, while the main contribution to the total mass comes from remnants of higher-mass stars.

We therefore investigate what is known about more metal-rich populations and somewhat arbitrarily apply the results to the metal-poor spheroid. After a lengthy review of the available evidence (which seems to indicate either a substantial variation in intermediate-mass MFs or substantial errors in their measurement) Scalo (1998) says “[i]f forced to choose an IMF for use in galactic evolution studies, I

would suggest” $\alpha = -1.7 \pm 0.5$ for the range ($M_{\odot} < M < 10 M_{\odot}$). The \pm is intended to represent a dispersion of measured values rather than an error. Scalo (1998) recommends a slightly shallower slope ($\alpha = -1.3$) for higher masses, but this change is uncertain and has almost no impact on our estimate of the mass density. For simplicity, we therefore adopt $\alpha = -1.7$ for $M > M_{\odot}$.

The slope must change somewhere below $1 M_{\odot}$ because at low masses ($M < 0.6 M_{\odot}$) and after correcting for binaries, several studies in different environments all find a flat MF, $\alpha \sim 0$ (Paper IV; Reid & Gizis 1997; Scalo 1998; Holtzman et al. 1998), although different authors argue for different break points. In Paper IV, we found a break at $M \sim 0.6 M_{\odot}$ from *HST* counts of disk M dwarfs. Significantly, however, this break point coincides with the boundary between our own M dwarf data and the MF for higher mass stars derived by Wielen, Jahreiß, & Krüger (1983) from stars within 20 pc. Reid & Gizis (1997) argue that their 8 pc sample is intrinsically cleaner than the 20 pc sample of Wielen et al. (1983) and find that the MF is flat all the way up to $1 M_{\odot}$. Scalo (1998) also adopts $1 M_{\odot}$ as the break point. However, Holtzman et al. (1998) find that the LF of Galactic bulge stars in Baade’s Window is very similar to the local disk LF derived in Paper IV (including the higher-mass data from Wielen et al. 1983) and thus also derive a similar MF. For simplicity, we adopt a break at the last point of our observations, that is $\alpha = -1.7$ for $M > 0.71 M_{\odot}$ and $\alpha = 0.25 M_{\odot}$ for $M < 0.71 M_{\odot}$. In fact, our final results do not depend strongly on the exact point of the transition.

5.2.1 Mass Density Without Correction for Binaries

Taking equation (4.12) at face value, the local mass density of the spheroid within the observed mass range $0.09 < M/M_{\odot} < 0.71$ is

$$\rho_{\text{obs}} = (2.86 \pm 0.92) \times 10^{-5} M_{\odot} \text{pc}^{-3} \quad (0.09 < M/M_{\odot} < 0.71), \quad (5.2)$$

Extending equation (4.12) into the brown dwarf regime, we find that the total substellar density is $\rho_{bd} = 0.23 \times 10^{-5} M_{\odot}$. This is an order of magnitude smaller than the stellar component of the spheroid evaluated in equation (5.2). The statistical errors are more than 50%. However, the important point is that substellar objects do not make a major contribution to the spheroid mass density unless the slope of the mass function changes sharply at the hydrogen-burning limit.

Using equation (5.1), we find the total mass of stars in the range $0.71 < M/M_{\odot} < 0.9$ is $\rho_{to} = 0.84 \times 10^{-5} M_{\odot} \text{pc}^{-3}$. Thus, the mass density of hydrogen-burning spheroid stars is $\rho_{hb} = \rho_{\text{obs}} + \rho_{to} = (3.7 \pm 1.0) \times 10^{-5} M_{\odot} \text{pc}^{-3}$, which can be compared to the value obtained by Bahcall, Schmidt, & Soneira (1983) of $\rho_{hb} = (4 - 14) \times 10^{-5} M_{\odot} \text{pc}^{-3}$.

Since the great majority of remnants are white dwarfs, we adopt $M = 0.6 M_\odot$ for all of the remnants of progenitors $M > 0.9 M_\odot$. We find a remnant mass density $\rho_{wd} = 1.3 \times 10^{-5} M_\odot \text{pc}^{-3}$, and hence a total mass density

$$\rho_{\text{tot}} = 5.2 \times 10^{-5} M_\odot \text{pc}^{-3}. \quad (5.3)$$

The statistical errors associated with this estimate are about 50%, but the largest sources of uncertainty are the arbitrary assumptions used to extend the mass function.

We note that had we chosen to break the power law at $1 M_\odot$ rather than at $0.71 M_\odot$, the contribution of more massive stars and remnants would have increased from $\rho_{to} + \rho_{wd} = 2.1 \times 10^{-5} M_\odot \text{pc}^{-3}$ to $3.5 \times 10^{-5} M_\odot \text{pc}^{-3}$. This would imply a 27% increase in the overall density.

5.2.2 Correction for Binaries

We are not aware of any data on the binary fraction for spheroid M dwarfs. We therefore somewhat arbitrarily adopt a correction similar to the one we derived for disk M dwarfs (Paper IV). For stars ($M < 0.71 M_\odot$), we decrease (steepen) the power law by 0.35 to $\alpha = -0.10$, and we fix the normalization at $0.71 M_\odot$ to the uncorrected density. This yields

$$\frac{dN}{d \log M} = 12.5 \times 10^{-5} \left(\frac{M}{0.71 M_\odot} \right)^{-0.1} \text{pc}^{-3} \quad (M < 0.71 M_\odot), \quad (5.4)$$

For higher masses, we continue to use equation (5.1).

We then find in units of $10^{-5} M_\odot \text{pc}^{-3}$, $\rho_{\text{obs}} = 3.6$, $\rho_{bd} = 0.7$, $\rho_{to} = 0.8$, and $\rho_{wd} = 1.3$. That is, the total density,

$$\rho_{\text{tot}} = 6.4 \times 10^{-5} M_\odot \text{pc}^{-3} \quad (\text{including binaries}), \quad (5.5)$$

is only about 25% higher than the uncorrected result. For comparison, the ‘‘heavy spheroid’’ model of Caldwell & Ostriker (1981) predicts a local density of $111 \times 10^{-5} M_\odot \text{pc}^{-3}$.

Fuchs & Jahreiß (1998) have obtained a lower limit to the local mass density of spheroid subdwarfs of $1 \times 10^{-4} M_\odot \text{pc}^{-3}$ using reliable Hipparcos parallaxes of stars in the Fourth Catalog of Nearby Stars (CNS4, Jahreiß & Wielen 1997) for a somewhat broader range of subdwarfs than we consider here. We can compare our result of $\rho_{\text{obs}} = 3.6 \times 10^{-5} M_\odot \text{pc}^{-3}$ with that of Fuchs & Jahreiß (1998) as follows. We count stars from their Table 1 in the range $0.09 < M/M_\odot < 0.71$ and in order to guard against contamination by the intermediate population, we select

only stars with velocities $V_T > 220 \text{ km s}^{-1}$. We then divide by the completeness factor of 0.53 (see § 4.3.2, but note that the factor differs very slightly because of slightly different geometries of the sample). This procedure yields 4 stars with total mass $M_{\text{tot}}/0.53 = 2.1 M_{\odot}$ within 25 pc or $(3.2 \pm 1.8) \times 10^{-5} M_{\odot} \text{ pc}^{-3}$. We note that there are two additional spheroid stars lurking at 25.5 pc (B. Fuchs & H. Jahreiß 1998, private communication) just beyond the 25 pc distance limit of the CNS4 catalog, which would raise the density to $(4 \pm 2) \times 10^{-5} M_{\odot} \text{ pc}^{-3}$. These lower limits are consistent within the errors with our estimate for the observed density $\rho_{\text{obs}} = 3.6 \times 10^{-5} M_{\odot} \text{ pc}^{-3}$.

The local normalization of the dark halo is $\rho_{\text{halo}} \sim 9 \times 10^{-3} M_{\odot} \text{ pc}^{-3}$. Of order half of this value may be in the form of compact objects now being detected in microlensing observations toward the LMC (Alcock et al. 1997). Thus, the spheroid contributes only $\sim 1\%$ of the observed microlensing optical depth.

If, as we discussed in § 4.3.4, the spheroid is composed of two components, one highly flattened and one roughly spherical, then our results would be sensitive only to the latter. In this case, the local density would be higher by a factor $\sim 5/3$. This higher density would not affect the spheroid’s microlensing optical depth, however, because the flattened component would not contribute significantly to microlensing.

Acknowledgements: This paper benefits greatly from conversations and correspondence sparked by its appearance as a preprint. Conard Dahn and Neill Reid (before he became referee) independently pointed out an important computational error in the renormalization of the DLHG LF. Ivan King drew our attention to the work of Capaccioli et al. Isabelle Baraffe and Gilles Chabrier helped clarify several issues related to theoretical isochrones. We are grateful to Conard Dahn and Isabelle Baraffe for making available some of their work in advance of publication. Finally, we are indebted to Neill Reid for a very thorough and helpful referee report. A. G. was supported in part by NSF grant AST 9420746 and in part by NASA grant NAG5-31111. J. N. B. was supported by NASA grant NAG5-1618. The work is based in large part on observations with the NASA/ESA Hubble Space Telescope, obtained at the Space Telescope Science Institute, which is operated by the Association of Universities for Research in Astronomy, Inc. (AURA), under NASA contract NAS5-26555. Important supplementary observations were made at KPNO and CTIO operated by AURA.

REFERENCES

1. Alcock, C., et al. 1997, ApJ, 486, 697
2. Bahcall, J. N. 1986, ARA&A, 24, 577
3. Bahcall, J. N., & Casertano, S. 1986, ApJ, 308, 347
4. Bahcall, J. N., Flynn, C., Gould, A., & Kirhakos, S. 1994, ApJ, 435, L51 (Paper I)
5. Bahcall, J. N., Kirhakos, S., Saxe, D. H., & Schneider, D. P. 1997, ApJ, 479, 642
6. Bahcall, J. N., Schmidt, M., & Soneira, R. M. 1983, ApJ, 265, 730
7. Bahcall, J. N. & Soneira, R. M. 1980, ApJS, 44, 73
8. Baraffe, I., & Chabrier, G. 1996, ApJ, 461, L51
9. Baraffe, I., Chabrier, G., Allard, F., & Hauschildt, P. H. 1995, ApJ, 446, L35
10. Baraffe, I., Chabrier, G., Allard, F., & Hauschildt P. H. 1997, A&A, 327, 1057
11. Beers, T. & Sommer-Larsen, J., 1995, ApJS, 96, 175
12. Caldwell, J. A. R. & Ostriker, J. P. 1981, ApJ, 251, 61
13. Capaccioli, M., Piotto, G., & Stiavelli, M. 1993, MNRAS, 261, 819
14. Casertano, S., Ratnatunga, K. U., & Bahcall, J. N. 1990, ApJ, 357, 435
15. Chabrier, G., & Méra, D. 1997, A&A, 328, 83
16. Chiba, M. & Yoshii, Y. 1998, AJ, 115, 229
17. Dahn, C. C., Liebert, J. W., Harris, H., & Guetter, H. C. 1995, p. 239, An ESO Workshop on: the Bottom of the Main Sequence and Beyond, C. G. Tinney ed. (Heidelberg: Springer)
18. D'Antona, F., & Mazzitelli, I. 1996, ApJ, 456, 329
19. Eggen, O. J. 1979a, ApJS, 39, 89
20. Eggen, O. J. 1979b, ApJ, 230, 786
21. Eggen, O. J. 1983, ApJS, 43, 457
22. Flynn, C. & Gould, A., & Bahcall, J. N., 1996, ApJ, 466, L55 (Paper II)
23. Fuchs, B. & Jahreiß, H. 1998, A&A, 329, 81
24. Gilmore, G. 1989, ARA&A, 27, 555
25. Gizis, J. E. 1997, AJ, 113, 806
26. Gould, A., Bahcall, J. N., & Flynn, C. 1996, ApJ, 465, 759 (Paper III)

27. Gould, A., Bahcall, J. N., & Flynn, C. 1997, ApJ, 482, 913 (Paper IV)
28. Graff, D. S. & Freese, K. 1996, ApJ, 456, L49
29. Harris, W. E. 1976, AJ, 81, 1095
30. Hartwick, R. D. A. 1987, in The Galaxy, G. Gilmore and B. Carswell, eds., p. 281 (Dordrecht: Reidel)
31. Hartwick, R. D. A. & Schade, D. 1990, ARA&A, 28, 437
32. Henry, T. J., & McCarthy, D. W. Jr. AJ, 106, 773
33. Holtzman, J. A., Watson, A. M., Baum, W. A., Grillmair, C. J., Groth, E. J., Light, R. M., Lynds, R., & O'Neil, E. J. 1998, AJ, in press (astro-ph9801321)
34. Jahrei, H. & Wielen, R., 1997, in: Presentation of the HIPPARCOS and TYCHO catalogues, eds. M.A.C. Perryman, P.L. Bernacca, ESA-SP 402, (Nordwijk:ESTEC)
35. Jones, J. B., Driver, S. P., Phillipps, S, Davies, J. I., Morgan, I., & Disney, M. J. 1997, A&A, 318, 729
36. Kinman, T. D., Wirtanen, C. A., & Janes, K. A. 1965, ApJS, 11, 223
37. Kroupa, P., Tout, C. A., & Gilmore, G. 1993, MNRAS, 262, 545
38. Laird, J. B., Carney, B. W., Rupen, M. P., & Latham, D. W. 1988, 96, 108
39. Layden, A. C., Hanson, R. B., Hawley, S. L., Klemola, A. R., Hanley, C. J. 1996, AJ, 112 2110
40. Liebert, J., Dahn, C. C., & Monet, D. G. 1988, ApJ, 332, 891
41. Lowenthal, J. D., Koo, D. C., Guzman, R., Gallego, J., Phillips, A. C., Faber, S. M., Vogt, N. P., Illingworth, G. D., & Gronwall, C. 1997, ApJ, 481, 673
42. Morrison, H. 1993, AJ, 106, 587
43. Mendez, R. A., Minniti, D., De Marchi, G., Baker, A., & Couch, W. J. 1997, MNRAS 283, 666
44. Mera, D., Chabrier, G., & Schaeffer, R. 1996, Europhys. Lett., 33, 327
45. Nissen, P. E. & Schuster, W. J. 1991, A&A, 251, 457
46. Piotto, G., Cool, A. M., & King, I. R. 1997, AJ, 113, 1345
47. Popowski, P. & Gould, A. 1998, ApJ, submitted (astro-ph 9802168)
48. Preston, G. W., Schectman, S. A., & Beers, T. C. 1991, ApJ, 375,121
49. Reid, I. N. & Gizis, J. E. 1997, AJ, 113, 2246
50. Reid, I. N., Hawley, S. L., & Gizis, J. E. 1995, AJ, 110, 1838

51. Reid, I. N., Yan, L., Majewski, S., Thompson, I., & Smail, I. 1996, *AJ*, 112, 1472
52. Reid, M., J. 1993, *ARA&A*, 31, 345
53. Richer, H. B. & Fahlman, G. G. 1992, *Nature*, 358, 383
54. Scalo, J. A. 1998, in *The Stellar Initial Mass Function Proceedings of the 38th Herstmonceux Conference*, eds. G. Gilmore, I. Parry, and S. Ryan, in press
55. Schmidt, M. 1975, 202, 22
56. Sommer-Larsen, J. & Zhen, C. 1990, *MNRAS*, 242, 10
57. Stiavelli, M., Piotto, G., Capaccioli, M., & Ortolani, S. 1991, in Janes K., ed., *Formation and Evolution of Star Clusters*, p. 449 (Boston, ASP)
58. Steidel, C., Giavalisco, M., Dickenson, M., & Adelberger, K. L. 1996, *AJ*, 112, 352
59. Stobie, R. S., Ishida, K., & Peacock, J. A. 1989, *MNRAS*, 238, 709
60. Wielen, R., Jahreiß, H., & Krüger, R. 1983, *IAU Coll. 76: Nearby Stars and the Stellar Luminosity Function*, A. G. D. Philip and A. R. Upgren eds., p 163
61. Zinn, R. 1985, *ApJ*, 293, 424